A Ridge-based Approach for Extraction and Visualization of 3D Atmospheric Fronts

Anne Gossing[1*] Andreas Beckert[2] Christoph Fischer[2] Nicolas Klenert[1] Vijay Natarajan[3,1]
George Pacey[4] Thorwin Vogt[2] Marc Rautenhaus[2] Daniel Baum[1]

[1]Zuse Institute Berlin [2]Universität Hamburg [3]Indian Institute of Science Bangalore [4]Freie Universität Berlin

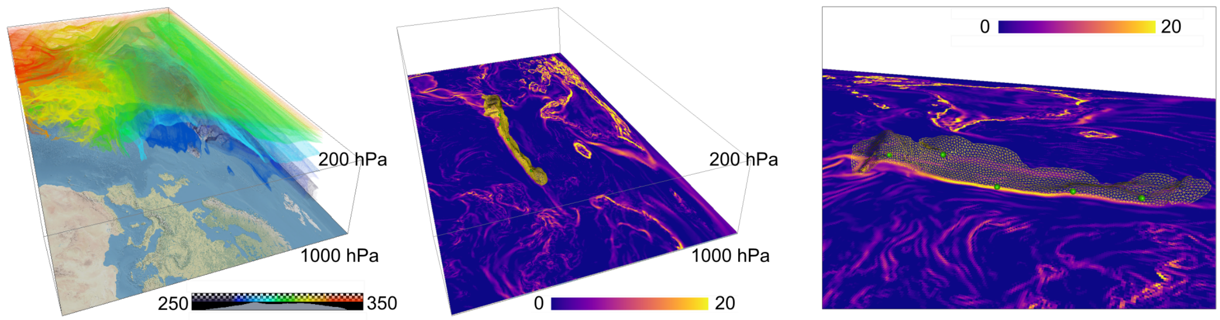

Figure 1: Atmospheric front represented as a ridge surface. (**left**) Profile of θ_E (equivalent potential temperature in Kelvin) over North Atlantic and Europe on 18 January 2018, 12:00 UTC. Warmer colors correspond to warm and moist air, cooler colors correspond to cold and dry air. A polar cold air mass encounters a subtropical warm air mass, resulting in the formation of a region with a high gradient of θ_E between them. (**middle**) Scalar field of the horizontal gradient magnitude of θ_E (in Kelvin per 100 km) and the extracted surface along the maximum gradient of the polar front. (**right**) Same as middle image but rotated and zoomed to the extracted surface.

Abstract

An atmospheric front is an imaginary surface that separates two distinct air masses and is commonly defined as the warm-air side of a frontal zone with high gradients of atmospheric temperature and humidity (Fig. 1, left). These fronts are a widely used conceptual model in meteorology, which are often encountered in the literature as two-dimensional (2D) front lines on surface analysis charts. This paper presents a method for computing three-dimensional (3D) atmospheric fronts as surfaces that is capable of extracting continuous and well-confined features suitable for 3D visual analysis, spatio-temporal tracking, and statistical analyses (Fig. 1, middle, right). Recently developed contour-based methods for 3D front extraction rely on computing the third derivative of a moist potential temperature field. Additionally, they require the field to be smoothed to obtain continuous large-scale structures. This paper demonstrates the feasibility of an alternative method to front extraction using ridge surface computation. The proposed method requires only the second derivative of the input field and produces accurate structures even from unsmoothed data. An application of the ridge-based method to a data set corresponding to Cyclone *Friederike* demonstrates its benefits and utility towards visual analysis of the full 3D structure of fronts.

Index Terms: Atmospheric front, ridge surface, visual analysis.

1 Introduction

The conceptual model of atmospheric fronts is widely used in meteorology to analyze mid-latitude weather dynamics. Weather fronts are drivers of precipitation in the mid-latitudes, with 50% (and locally up to 90%) of extreme precipitation events occurring at or in proximity to a front [7]. Frontal environments favor the occurrence of atmospheric convection [6, 8, 14, 26], emphasizing the importance of enhancing the meteorological community's understanding of interactions between frontal regions and small-scale atmospheric processes such as convective cells. In the literature fronts are most often encountered as 2D front lines on surface analysis charts. However, since convection includes vertical movement, investigations of front-convection interactions require a 3D representation of the front. In three dimensions, front lines become imaginary surfaces that separate two air masses with distinct characteristics, commonly defined as the warm-air side of a *frontal zone* with high gradients of atmospheric temperature and humidity [15]. They can thus be understood as interfaces between those two air masses [25]. As a synoptic-scale phenomenon, frontal surfaces have typical length scales on the order of 1000 km, whereas the width of the frontal zone is usually two orders of magnitude smaller.

Feature extraction algorithms have been proposed to automatically detect atmospheric fronts; most of them work with 2D data [11, 16, 17]. Only recently, advances for extracting full 3D structures of fronts have been made, with pioneering work including the approach by Kern et al. [12], which was later further developed by Beckert et al. [3]. Their method for detecting and visualizing 3D frontal structures is, to the best of our knowledge, the only one currently available. However, one characteristic of this method is that horizontal smoothing of the input data must be employed to obtain visually continuous features on synoptic scales. On such length scales, smoothing is acceptable since the focus is on the large-scale structure. In addition, this approach [3, 12] requires the third derivative to be computed, which may also become prone to numerical instabilities for highly resolved datasets. 3D visualization of atmospheric fronts allows analysis of the atmospheric dynamical and thermodynamic structure that would not be possible with 2D methods, for example, by analyzing frontal tilt and its association with convective processes [3, 12].

The overall motivation of our work is the investigation of scale interactions during the formation of atmospheric convection in

*e-mail: gossing@zib.de

frontal environments. Therefore, it is necessary to obtain a method capable of extracting continuous and well-confined 3D frontal features suitable for visual analysis, spatio-temporal tracking, and statistical analyses. To preserve small-scale convective processes, smoothing is prohibitive.

In this paper, we propose an alternative approach [13] for extracting atmospheric fronts without the requirement of data smoothing. It is based on ridge surface detection and can extract 3D frontal surfaces based on the second derivative of a moist potential temperature field. We show that extracting frontal structures as ridge surfaces using the method of Klenert et al. [13] leads to accurate and robust representations of fronts, while maintaining the original data resolution. We demonstrate the advantages of the proposed approach via experiments on data corresponding to Cyclone *Friederike*. A comparison of the results with the state-of-the-art contour-based method [3] shows an improvement in accuracy.

2 Related work

Visualizations are key for facilitating the interpretation of complex meteorological data, enabling deeper insights into weather patterns and atmospheric phenomena [19]. For atmospheric fronts, visualization techniques are usually based on ridge detection and frontal features in two dimensions [10].

A common approach to front detection [10] in atmospheric sciences uses the third derivative of thermal variables to detect the horizontal warm-air "boundaries" of frontal zones, *i.e.*, regions with a strong horizontal gradient of the thermal variable. Atmospheric front detection methods as described by Hewson [10] were primarily restricted to 2D. Detection, visualization, and interactive exploration of atmospheric fronts as surfaces in 3D became possible due to recently developed methods by Kern et al. [12] and Beckert et al. [3]. These methods are based on contour extraction from a scalar field and are available via the open-source framework Met.3D [20].

Feature extraction by calculating the ridge, valley, or crease surfaces is of significant interest for many visualization, graphics, and geometry processing applications and has been studied extensively [1, 2, 4, 5, 22]. There are broadly two approaches followed in the literature towards ridge extraction. One uses the Hessian to compute crease surfaces [2, 22]. The second approach is based on computing optimal paths [23] to project ridge surface patches in a volume onto a ridge curve on the boundary of the volume [4, 5]. Algarni and Sundaramorthi [1] and Klenert et al. [13] employed the second approach, resulting in surfaces that are more stable under noise. Klenert et al. [13] further guarantee that the resulting surface is an orientable manifold. This algorithm was developed specifically in the context of extracting thin layers of ancient papyrus rolls and is optimized for speed by employing fast marching algorithms [23]. Here, we apply their ridge surface extraction algorithm [13] for extracting atmospheric fronts.

3 Extraction of frontal structures

Atmospheric frontal structures are 3D phenomena defined as a region of high temperature gradients and/or high humidity gradients. They are typically defined as surfaces because their characteristic length is one to two orders of magnitude greater than their width. In particular, the front surface is defined as a surface along the warm-side boundary of the frontal zone [21]. We follow this definition to extract and visualize the frontal structure as a surface along the warm-side boundary of the frontal zone.

Frontal zone and temperature gradient. Inside the frontal zone, the temperature horizontally increases more rapidly than outside (Fig. 2, black line). The first partial derivative of temperature increases across the cold-side boundary and decreases across the warm-side boundary, attaining a maximum within the zone (Fig. 2, yellow line). The boundaries of the zone are defined as the surfaces containing the inflection points of the first partial derivative. In other words, the second derivative of the temperature field increases to a maximum on the cold-side boundary and decreases to a minimum on the warm-side boundary (Fig. 2, blue line), corresponding to zero points of the third derivative (Fig. 2, red line). Hence, the front is often defined and extracted as the collection of points where the third derivative of the temperature field is zero and the second derivative is negative [10]. This collection of zero points may be extracted using an isocontour extraction algorithm, resulting in a set of candidate surfaces. These candidates need filtering based on multiple complex criteria to extract the frontal surface.

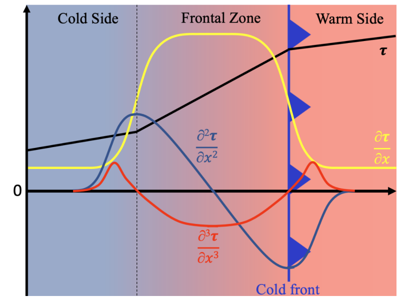

Figure 2: Illustration of a straight weather front. The frontal zone is characterized by a sharp gradient of the thermal parameter τ (black). The gradient (yellow) experiences a significant change on the boundary, corresponding to an extremum in the second derivative (blue) and a zero point of the third derivative of τ (red). The ridge extraction method uses the magnitude of the minimum of the second derivative for extracting the warm-side boundary surface. Additionally, the ridge method can be used to extract the surface along the steepest gradient of τ, which is a stable feature inside of the frontal zone. Figure adapted from Beckert et al. [3].

We propose to compute the front surface directly from the second derivative and without requiring additional filtering steps. Specifically, we will compute the frontal structure by applying a method originally developed for extracting 2D manifolds representing thin-layer structures in folded papyrus sheets [13]. This is an interactive method to extract ridge surfaces from three-dimensional datasets.

Ridge-based frontal surface. A ridge surface of a 3D scalar field is a surface that contains all local maxima of the field with respect to the surface normal. Two key ideas are required to construct such a surface with a guarantee of producing an orientable 2-manifold.

First, the fast marching algorithm [23] is used to compute the ridge surface from the scalar field of the second derivative, thereby avoiding the computation of the third derivative and its zeros to locate the ridge points. Fast marching is an algorithm that computes the minimum time required for a *wavefront* to reach each point in the domain beginning from a set of *seed* points. The term *wavefront* refers to the conceptual interface or boundary of a region that is evolving through the spatial domain and is not related to the weather front. The marching is directed by a cost function, which favors larger values and assigns unlimited 'speed' to maxima, while minima are assigned with zero 'speed'. Terminating the fast marching algorithm at a specific moment allows us to identify a volume containing all points that can be reached at that time. Hence, the boundary of this volume represents an isosurface with an isovalue of the latest, and therefore highest, computed time. Those times are recorded, resulting in a time field. An *optimal path* of the fast marching method refers to the path taken by a point on the wavefront, and coincides with the integral curves of this time field.

The second idea is to utilize the optimal paths of the fast marching algorithm to reformulate the ridge surface extraction

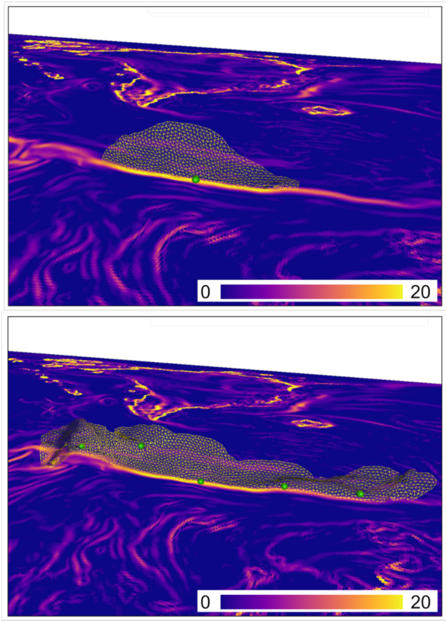

Figure 3: Illustration of the ridge surface extraction algorithm [13] applied on the gradient magnitude field of the wet-bulb potential temperature [K/100 km] of the Cyclone *Friederike*. The gradient magnitude field is visualized using a color map, the seed points are shown in green, and the extracted surface is shown as a triangle mesh. (**top**) The first seed point is specified manually within the area of high gradient magnitude. The corresponding surface patch is generated according to a user-specified maximum distance. (**bottom**) Additional seed points are generated automatically in subsequent iterations within the surface patch computed in a previous iteration. All surface patches are merged into a ridge surface representing the maximum gradient in the frontal zone.

problem as one of computing a ridge curve on the isosurface. Thus, a three-dimensional problem is temporarily reduced to a two-dimensional problem. Executing this simpler task of computing a ridge curve within a surface followed by a step that projects the curve back into the 3D domain to compute a patch of the ridge surface results in a method that is more stable under noise. Algarni and Sundaramorthi [1] showed that the optimal paths of the fast marching method are contained within the ridge surface. Klenert et al. [13] improved this method and additionally calculated a distance field, representing the length of optimal paths from the seed points to any given domain point. Thus, given an isosurface of the time field and assuming the desired ridge surface intersects the chosen isosurface, the ridge curve on the isosurface with respect to the distance field is also contained in the ridge surface.

Computation. The ridge extraction algorithm begins with a set of seed points that are assumed to be on or near the desired surface. A time and distance field is computed for each seed point within its spatial neighborhood by applying the fast marching method. The fast marching algorithm iteratively tracks the interface of an evolving region and terminates upon reaching a predefined distance from the seed point. This distance is determined as the length of the computed optimal paths as opposed to a simple Euclidean distance. The interface or boundary of the neighborhood region corresponds to an isosurface of the time field. After computing the neighborhood region, its boundary surface is partitioned into two surface segments. The shared boundary curve of the two segments is a closed ridge curve lying on the time isosurface. In the next step, the labels associated with the two segments are projected onto the neighborhood region. The interface surface between the two labels determines a ridge surface patch. Essentially, each seed point generates a volume with two labels. Merging the label sets for all seed points and calculating a neighborhood relationship between the seed points allows the algorithm to generate a coherent ridge surface. For our use cases, computing the ridge surface took only a few seconds. The extraction procedure is illustrated in Fig. 3. The approach also supports automated seed point generation. Regions of higher distances are the favored locations for the placement of additional seed points, whereas shorter distances serve as a stopping condition.

4 Data

For this study, we use ERA5 [9] global reanalysis data. The data is horizontally interpolated onto a regular grid with a grid point spacing of 0.25° in both latitude and longitude. Vertically, 137 model levels are interpolated to constant pressure levels at 10 hPa intervals. We used the variables temperature, specific humidity, and pressure to derive the thermal quantities equivalent potential temperature θ_E and wet-bulb potential temperature θ_W. Both variables conserve temperature under pressure changes and moist processes in the atmosphere. In particular, they are suitable to extract continuous front features because strong gradients of humidity often occur along with high temperature gradients within frontal zones [25].

The ridge extraction algorithm takes as input a scalar field given by the magnitude of the horizontal gradient field of the thermal quantity $\|\nabla_h \tau\|_2$ or the magnitude of the horizontal gradient of this scalar field $\|\nabla_h \|\nabla_h \tau\|_2\|_2$. The former is used for extracting the maximum gradient surface lying within the frontal zone, the latter extracts the warm-air side boundary surface of the frontal zone.

The data corresponds to the case of the winter storm *Friederike* (Fig. 1). This data is also discussed by Beckert et al. [3], albeit with model levels in the vertical direction as opposed to levels of constant pressure used in this study. We consider the time step of 18 January 2018, 12 UTC. For additional visualizations of the winter storm and description of the data on this time step, we refer the reader to Figures 2, 5 and 12 in the paper by Beckert et al.

5 Results

We extract the warm-air side boundaries of atmospheric frontal zones as orientable 2-manifolds using the ridge surface method described in Sec. 3 and compare them with fronts extracted using the contour-based algorithm by Beckert et al. [3]. The ridge extraction method uses extrema of the second derivative of the thermal parameter, which corresponds to zeros of the third derivative that are used for front extraction by the contour-based methods. So, we expect results from both methods to be similar in terms of geographic location, up to some numerical error. Both methods are applied on the same θ_W fields. All derived data fields for ridge extraction were calculated in Met.3D and imported into Amira [24] for the extraction of the ridge surfaces. Fig. 4 shows the fronts extracted by both methods for the example of Cyclone *Friederike*, visualized in Met.3D [20].

Ridge-based fronts. In Fig. 4A, the ridge surface extraction method [13] is used to extract ridge structures from unsmoothed input data to visualize the two main frontal features of the domain (green surfaces). The left frontal structure forms an elongated, almost straight band from the Atlantic over France to Central Germany, representing the polar front shown in Fig. 1. The second front is a smaller curved band over Northern Germany and is associated with storm *Friederike* (low-pressure center is visible through the pressure contour lines). Since no filtering except for the optimal path length criterion (cf. Sec. 3) is applied on these surfaces, they appear solid and continuous, with high local curvature reflecting the structure of the underlying variable field.

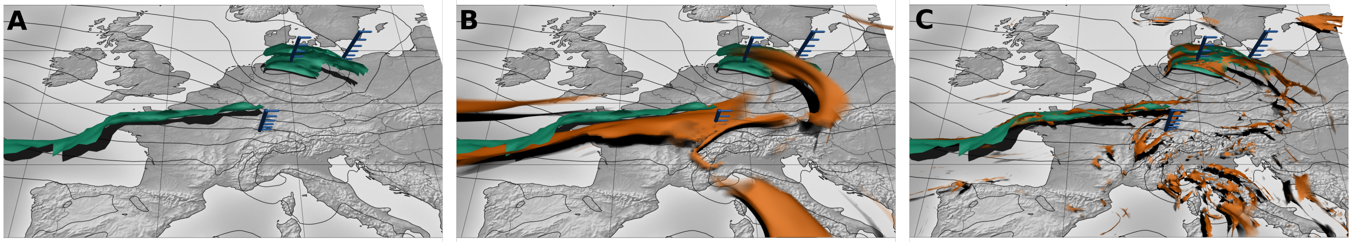

Figure 4: Frontal surfaces (warm-air sides of frontal zones) extracted from the wet-bulb potential temperature θ_W during Cyclone *Friederike* (18 January 2018 12:00 UTC). (A) Front surfaces extracting using the ridge-based method from the θ_W field without smoothing. (B,C) Overlay of fronts extracted using the ridge-based method (green) and contour-based method (orange). The contour-based method is applied on the θ_W field after smoothing (smoothing radius 100 km) in (B) and is applied without prior smoothing in (C). The geometric extent of the features should only be compared qualitatively, as different methods for filtering were used. Blue vertical axis aids spatial perception.

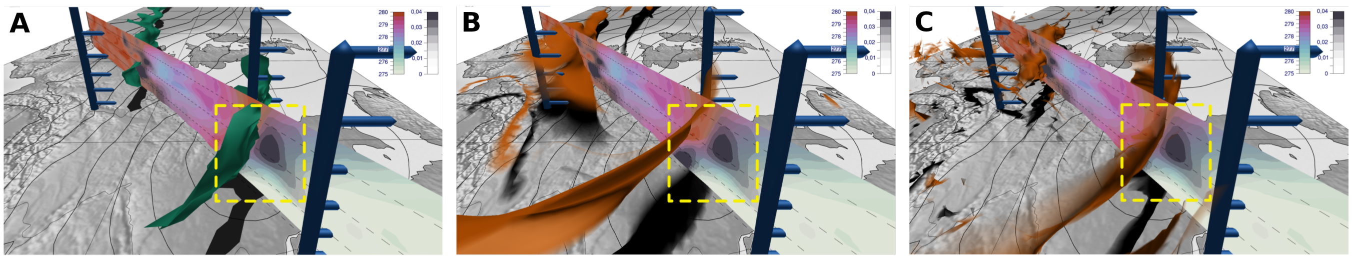

Figure 5: Frontal surfaces (warm-air sides of frontal zones) extracted using (A) our ridge-based method from θ_W without smoothing, (B) contour-based method from θ_W after smoothing, and (C) contour-based method from θ_W without smoothing. These surfaces are the same as in Fig. 4, but viewed looking westward over northern Germany towards the North Atlantic. The vertical section shows unsmoothed θ_W (K, blue-to-red color bar) and $\|\nabla_h \theta_W\|_2$ (K (100 km)$^{-1}$, gray color bar). The yellow box highlights the region of interest discussed in the text.

Contour-based fronts. In Fig. 4B, the ridge surface structures of Fig. 4A (green surfaces) are visualized together with the frontal visualizations of the contour-based method [3] generated from smoothed input data for the entire domain (orange surfaces). The orange surfaces were smoothed over a length scale of 100 km and the following filter parameters were applied: (1) thermal front parameter (TFP) of 0.3–0.5 K (100 km)$^{-2}$; (2) frontal strength of θ_W of 0.8–1.2 K (100 km)$^{-1}$; (3) frontal strength of dry potential temperature θ of 0.8–1.2 K (100 km)$^{-1}$. The contour-based method essentially captures the same two main features, with additional features along the Alps (likely a stationary front due to topography), along the west coast of Italy, and north of the polar front. This method produces straighter bands, leading to a positional difference of several tens of kilometers between the methods, especially where ridge surfaces are curved.

Data smoothing. Fig. 4C shows the effect of data smoothing for the contour-based method in comparison with Fig. 4B, where no smoothing was used. The following filter settings [3, Sec. 2] are used to receive the contour-based front structures: (1) TFP of 2.5–3.0 K (100 km)$^{-2}$; (2) frontal strength of θ_W of 2.0–3.0 K (100 km)$^{-1}$; (3) frontal strength of dry potential temperature θ (to filter orographic fronts) of 1.0–1.5 K (100 km)$^{-1}$. As can be observed, using unsmoothed data leads to multiple small patches (orange) instead of continuous bands. However, those patches are well aligned with the extracted ridge surfaces. The frontal structure north of the polar front disappears, while the previously continuous bands over the Alps and Italy appear as clusters of patches.

Fig. 5 examines selected details of the frontal structures more closely, using a vertical section showing θ_W and its gradient that cuts through both fronts. The view is looking westward over Northern Germany towards the North Atlantic. The frontal surfaces extracted by both methods and computed from the unsmoothed θ_W fields align well with the warm-air side of the frontal zone (Fig. 5A and C; gray shaded region on the vertical section, *i.e.*, where $\|\nabla_h \theta_W\|_2$ is largest). Fig. 5B shows that the smoothed front visualization is not aligned with the boundary of the frontal zone. Applying a smoothing radius of 100 km, which is on the same length scale as the width of a frontal zone, can lead to local deviations in the front's localization that may be on the order of one magnitude of the frontal zone. Thus, smoothing potentially impacts the analysis of small-scale processes in frontal environments.

6 Conclusions

We presented a novel method for computing 3D atmospheric fronts which results in stable features that enable subsequent investigations of frontogenesis, evolution, and morphology. To the best of our knowledge, this is the first 3D atmospheric front extraction method based on a ridge extraction approach. Compared to existing front extraction methods, our approach generates stable, continuous structures without the need for data smoothing, thereby enhancing the accuracy of front representations. This potentially allows for straightforward application in challenging datasets with strong fluctuations, such as those where small-scale convective processes disturb the frontal zone. By depending only on the second derivative rather than the third, our approach reduces the numerical error and ensures robust results. Particularly in cases where analyzing the maximum gradient of θ_W within the frontal zone is of interest, our use of the first derivative further strengthens the reliability of our results. However, analysis of further use cases is needed to support these findings. One limitation of the presented method is its requirement for seeding, the influence of which also needs further evaluation. In addition, quantitative evaluation of high-resolution data sets will be carried out to strengthen the analysis of the method. In the next phase of our research, we will utilize the extracted ridge surfaces to investigate scale interactions during the formation of atmospheric convection in frontal environments [18].

Acknowledgments

This research has been mainly funded by Deutsche Forschungsgemeinschaft (DFG, German Research Foundation) through grant CRC 1114 "Scaling Cascades in Complex Systems", grant Transregional CRC (TRR) 165 "Waves to Weather", and under Germany's Excellence Strategy – EXC 2037 "CLICCS - Climate, Climatic Change, and Society" (project number 390683824), as well as grant BA 5042/2-1. It was further supported by the Alexander von Humboldt Foundation and the cluster of excellence MATH+.

References

[1] M. Algarni and G. Sundaramoorthi. Surfcut: Surfaces of minimal paths from topological structures. *IEEE Trans. Pattern Anal. Mach. Intell.*, 41(3):726–739, Mar. 2019. doi: 10.1109/TPAMI.2018.2811810 2, 3

[2] S. Barakat and X. Tricoche. An image-based approach to interactive crease extraction and rendering. *Procedia Computer Science*, 1(1):1709–1718, May 2010. doi: 10.1016/j.procs.2010.04.192 2

[3] A. A. Beckert, L. Eisenstein, A. Oertel, T. Hewson, G. C. Craig, and M. Rautenhaus. The three-dimensional structure of fronts in mid-latitude weather systems in numerical weather prediction models. *Geoscientific Model Development*, 16(15):4427–4450, Aug. 2023. doi: 10.5194/gmd-16-4427-2023 1, 2, 3, 4

[4] F. Benmansour and L. D. Cohen. Fast object segmentation by growing minimal paths from a single point on 2d or 3d images. *Journal of Mathematical Imaging and Vision*, 33(2):209–221, Feb. 2009. doi: 10.1007/s10851-008-0131-0 2

[5] F. Benmansour and L. D. Cohen. From a single point to a surface patch by growing minimal paths. In *Proceedings of the Second International Conference on Scale Space and Variational Methods in Computer Vision*, SSVM '09, p. 648–659. Springer-Verlag, Berlin, Heidelberg, 2009. doi: 10.1007/978-3-642-02256-2_54 2

[6] K. A. Browning and T. W. Harrold. Air motion and precipitation growth at a cold front. *Quarterly Journal of the Royal Meteorological Society*, 96(409):369–389, July 1970. doi: 10.1002/qj.49709640903 1

[7] J. L. Catto and S. Pfahl. The importance of fronts for extreme precipitation. *Journal of Geophysical Research: Atmospheres*, 118(19):10,791–10,801, 2013. doi: 10.1002/jgrd.50852 1

[8] A. H. Fink, T. Brücher, V. Ermert, A. Krüger, and J. G. Pinto. The European storm Kyrill in January 2007: Synoptic evolution, meteorological impacts and some considerations with respect to climate change. *Natural Hazards and Earth System Sciences*, 9(2):405–423, Mar. 2009. doi: 10.5194/nhess-9-405-2009 1

[9] H. Hersbach, B. Bell, P. Berrisford, S. Hirahara, A. Horányi, J. Muñoz-Sabater, J. Nicolas, C. Peubey, R. Radu, D. Schepers, A. Simmons, C. Soci, S. Abdalla, X. Abellan, G. Balsamo, P. Bechtold, G. Biavati, J. Bidlot, M. Bonavita, G. De Chiara, P. Dahlgren, D. Dee, M. Diamantakis, R. Dragani, J. Flemming, R. Forbes, M. Fuentes, A. Geer, L. Haimberger, S. Healy, R. J. Hogan, E. Hólm, M. Janisková, S. Keeley, P. Laloyaux, P. Lopez, C. Lupu, G. Radnoti, P. de Rosnay, I. Rozum, F. Vamborg, S. Villaume, and J.-N. Thépaut. The ERA5 global reanalysis. *Quarterly Journal of the Royal Meteorological Society*, 146(730):1999–2049, 2020. doi: 10.1002/qj.3803 3

[10] T. D. Hewson. Objective fronts. *Meteorological Applications*, 5(1):37–65, 1998. doi: 10.1017/S1350482798000553 2

[11] J. Jenkner, M. Sprenger, I. Schwenk, C. Schwierz, S. Dierer, and D. Leuenberger. Detection and climatology of fronts in a high-resolution model reanalysis over the Alps. *Meteorological Applications*, 17(1):1–18, Mar. 2010. doi: 10.1002/met.142 1

[12] M. Kern, T. Hewson, A. Schäfler, R. Westermann, and M. Rautenhaus. Interactive 3d visual analysis of atmospheric fronts. *IEEE Transactions on Visualization and Computer Graphics*, 25(1):1080–1090, Jan. 2019. doi: 10.1109/TVCG.2018.2864806 1, 2

[13] N. Klenert, V. Lepper, and D. Baum. A local iterative approach for the extraction of 2d manifolds from strongly curved and folded thin-layer structures. *IEEE Transactions on Visualization and Computer Graphics*, 30(01):1260–1270, Jan. 2024. doi: 10.1109/TVCG.2023.3327403 2, 3

[14] K.-O. Lee, C. Flamant, V. Ducrocq, F. Duffourg, N. Fourrié, and S. Davolio. Convective initiation and maintenance processes of two back-building mesoscale convective systems leading to heavy precipitation events in southern italy during hymex iop 13. *Quarterly Journal of the Royal Meteorological Society*, 142(700):2623–2635, June 2016. doi: 10.1002/qj.2851 1

[15] J. E. Martin. *Mid-Latitude Atmospheric Dynamics*. Wiley-Blackwell, Hoboken, NJ, May 2006. 1

[16] S. Niebler, A. Miltenberger, B. Schmidt, and P. Spichtinger. Automated detection and classification of synoptic-scale fronts from atmospheric data grids. *Weather and Climate Dynamics*, 3(1):113–137, Feb. 2022. doi: 10.5194/wcd-3-113-2022 1

[17] S. Niebler, B. Schmidt, H. Tost, and P. Spichtinger. Automated identification and location of three dimensional atmospheric frontal systems. In J. Mikyška, C. de Mulatier, M. Paszynski, V. V. Krzhizhanovskaya, J. J. Dongarra, and P. M. Sloot, eds., *Computational Science – ICCS 2023*, Lecture Notes in Computer Science, pp. 3–17. Springer Nature Switzerland, Cham, 2023. doi: 10.1007/978-3-031-36021-3_1 1

[18] G. Pacey, S. Pfahl, and L. Schielicke. The interaction between cold fronts and convection in the mid-latitudes. vol. 18 of *EMS Annual Meeting*. Copernicus GmbH, June 2021. doi: 10.5194/ems2021-343 4

[19] M. Rautenhaus, M. Böttinger, S. Siemen, R. Hoffman, R. M. Kirby, M. Mirzargar, N. Rober, and R. Westermann. Visualization in meteorology—a survey of techniques and tools for data analysis tasks. *IEEE Transactions on Visualization and Computer Graphics*, 24(12):3268–3296, Dec. 2018. doi: 10.1109/TVCG.2017.2779501 2

[20] M. Rautenhaus, M. Kern, A. Schäfler, and R. Westermann. Three-dimensional visualization of ensemble weather forecasts – Part 1: The visualization tool Met.3D (version 1.0). *Geoscientific Model Development*, 8(7):2329–2353, July 2015. doi: 10.5194/gmd-8-2329-2015 2, 3

[21] R. J. Renard and L. C. Clarke. Experiments in numerical objective frontal analysis. *Monthly Weather Review*, 93(9):547–556, Sept. 1965. doi: 10.1175/1520-0493(1965)093<0547:EINOFA>2.3.CO;2 2

[22] T. Schultz, H. Theisel, and H.-P. Seidel. Crease surfaces: From theory to extraction and application to diffusion tensor MRI. *IEEE Transactions on Visualization and Computer Graphics*, 16(1):109–119, Jan. 2010. doi: 10.1109/TVCG.2009.44 2

[23] J. A. Sethian. Fast marching methods. *SIAM Review*, 41(2):199–235, Jan. 1999. doi: 10.1137/S0036144598347059 2

[24] D. Stalling, M. Westerhoff, and H.-C. Hege. Amira: a highly interactive system for visual data analysis. In *The Visualization Handbook*, pp. 749–767. Elsevier, 2005. 3

[25] C. M. Thomas and D. M. Schultz. Global climatologies of fronts, airmass boundaries, and airstream boundaries: Why the definition of "Front" matters. *Monthly Weather Review*, 147(2):691–717, Feb. 2019. doi: 10.1175/MWR-D-18-0289.1 1, 3

[26] T. Weusthoff and T. Hauf. The life cycle of convective-shower cells under post-frontal conditions. *Quarterly Journal of the Royal Meteorological Society*, 134:841–857, Apr. 2008. doi: 10.1002/qj.260 1